

# Lattice Gas Dynamics; Application to Driven Vortices in Two Dimensional Superconductors

Violeta Gotcheva, Albert T. J. Wang,\* and S. Teitel

*Department of Physics and Astronomy, University of Rochester, Rochester, NY 14627*

(Dated: November 19, 2018)

A continuous time Monte Carlo lattice gas dynamics is developed to model driven steady states of vortices in two dimensional superconducting networks. Dramatic differences are found when compared to a simpler Metropolis dynamics. Subtle finite size effects are found at low temperature, with a moving smectic that becomes unstable to an anisotropic liquid on sufficiently large length scales.

PACS numbers: 05.10.Ln, 74.25.Qt, 74.81.Fa

Keywords:

The nature of the driven steady states of many interacting particles, and the transitions between them, is a topic of much active interest. As with equilibrium systems, the use of lattice models, in which the degrees of freedom sit on the sites of a discrete grid, has led to analytical simplifications and greater accuracy in numerical simulations, as compared to continuum models. [1]. Here we consider lattice models applied to driven two dimensional (2D) charges on a triangular grid, as a model for vortices in a honeycomb superconducting network. We use two distinct lattice gas dynamics, both intended to model the overdamped diffusive limit: (i) the commonly used driven diffusive Metropolis Monte Carlo (MC) [2], and its modification to a (ii) driven diffusive continuous time Monte Carlo [3, 4]. We believe this is the first application of continuous time MC in the context of driven diffusive problems. We find that the steady states are qualitatively different for the two dynamics, and that the latter gives the more physically reasonable results. We find that finite size effects can be subtle at low temperature.

Our model is given by the Hamiltonian [5],

$$\mathcal{H} = \frac{1}{2} \sum_{i,j} (n_i - f)V(\mathbf{r}_i - \mathbf{r}_j)(n_j - f) , \quad (1)$$

where  $n_i = 0, 1$  is the charge on site  $\mathbf{r}_i$  of a periodic triangular grid,  $-f$  is a fixed uniform background charge, and  $V(\mathbf{r})$  is the 2D lattice Coulomb interaction as defined in Ref.[5] for a triangular grid with periodic boundary conditions. We take as grid basis vectors  $\hat{a}_1 = \hat{x}$ , and  $\hat{a}_2 = \frac{1}{2}\hat{x} + \frac{\sqrt{3}}{2}\hat{y}$ , the grid size is  $L_i$  in direction  $\hat{a}_i$ , and the grid sites are  $\mathbf{r} = m_1\hat{a}_1 + m_2\hat{a}_2$ ,  $m_i = 0, \dots, L_i - 1$ . Neutrality requires a fixed number of charges,  $\sum_i n_i \equiv N_c = fL_1L_2$ . In this work we use a charge density of  $f = 1/25$ . In equilibrium, this model is characterized by a single first order melting transition at  $T_m \simeq 0.009$  from a triangular commensurate pinned solid with long range translational order to an ordinary liquid [5].

We now consider behavior in a uniform driving force,  $\mathbf{F} = F\hat{x}$ , parallel to the grid direction  $\hat{a}_1$ . We con-

sider two different dynamics, both involving single particle moves only.

(i) Driven diffusive Metropolis Monte Carlo (DDMC) [2]: At each step of the simulation, a charge  $n_i = 1$  is selected at random, and moved a distance  $\Delta\mathbf{r}$  to a nearest neighbor site. If  $\hat{a}_3 \equiv \hat{a}_1 - \hat{a}_2$ , then  $\Delta\mathbf{r}$  is chosen randomly from the six possibilities,  $\pm\hat{a}_i$ ,  $i = 1, 2, 3$ . If  $\mathcal{H}_{\text{old}}$  and  $\mathcal{H}_{\text{new}}$  give the interaction energy (1) before and after the move, one computes,

$$\Delta E \equiv \mathcal{H}_{\text{new}} - \mathcal{H}_{\text{old}} - \mathbf{F} \cdot \Delta\mathbf{r} , \quad (2)$$

where the last term is the work done by the force on the moving charge. One accepts or rejects this move according to the usual Metropolis MC algorithm. One pass of  $N_c$  steps equals one unit of simulation time. Statistical averages are computed averaging over the generated configurations as in ordinary MC.

(ii) Driven diffusive continuous time Monte Carlo (CTMC) [3, 4]: At each step of the simulation, one considers the possible move of each charge  $n_i = 1$  in each of the six directions,  $\hat{\alpha} = \pm\hat{a}_i$ , computing the energy change  $\Delta E_{i\alpha}$  of each move according to Eq.(2). We take the rate for a particular move  $i\alpha$  to be,

$$W_{i\alpha} \equiv W_0 e^{-\Delta E_{i\alpha}/2T} , \quad (3)$$

where  $1/W_0$  sets the unit of time. The total rate for all single particle moves is then  $W_{\text{tot}} = \sum_{i\alpha} W_{i\alpha}$ . We decide which move to make by sampling the probability distribution  $P_{i\alpha} \equiv W_{i\alpha}/W_{\text{tot}}$ , and then update the simulation clock by  $\Delta t = 1/W_{\text{tot}}$ . Averages of an observable  $\mathcal{O}$  are computed as,

$$\langle \mathcal{O} \rangle = \frac{1}{\tau} \int \mathcal{O}(t) dt = \frac{1}{\tau} \sum_s \mathcal{O}_s \Delta t_s \quad (4)$$

where  $s$  labels the steps of the simulation,  $\mathcal{O}_s$  is the value of  $\mathcal{O}$  in the configuration at time  $t_s$ ,  $\Delta t_s \equiv t_{s+1} - t_s$ , and  $\tau \equiv \sum_s \Delta t_s$  is the total time of the simulation.

The CTMC, originally introduced as the “n-fold way” for spin models [3], owes its name to the continuous variations in the time steps  $\Delta t_s$ , which vary as the configu-

ration changes throughout the simulation. It is a *rejectionless* algorithm designed to speed up excitation over energy barriers at low temperatures; rather than waste many rejected moves until a rare acceptance takes one up an energy barrier, the energy barriers  $\Delta E$  themselves set the time scale for each move, which then happens in a single step. Simulation clock times can vary over orders of magnitude as  $T$  varies.

In CTMC, there are many possible choices for the rates that will obey local detailed balance. It can be shown [6] that the rates of Eq.(3) lead to ordinary Langevin dynamics in the limit  $\Delta E_{i\alpha}/T \ll 1$ . Our simulations, however, are generally in the opposite limit  $\Delta E_{i\alpha}/T \gtrsim 1$ . To see what physical limit this corresponds to, consider a single particle on a one dimensional grid in a driving force  $F$ . A simple calculation gives for the average velocity of the particle,  $\langle v \rangle = W_{\text{tot}} \tanh(F/2T) = 2W_0 \sinh(F/2T)$ . If we interpret the grid sites as the minima of a periodic pinning potential  $U(\mathbf{r})$  in the continuum, with energy barrier  $U_0$ , then  $W_0 \sim e^{-U_0/T}$  and the above velocity then describes motion in such a periodic potential in the limit  $F \lesssim U_0$  [7]. CTMC thus appears to describe the limit where motion is due to thermal activation over barriers; it is unclear if it can describe the very large drive limit, where the washboard potential  $U(\mathbf{r}) - \mathbf{F} \cdot \mathbf{r}$  loses its local minima parallel to  $\mathbf{F}$ . This large drive limit has been the subject of numerous theoretical [8, 9, 10] and numerical [11, 12, 13, 14] works for the case of random pinning.

In this paper we consider just the structural properties of the steady state. These are given by the structure function,

$$S(\mathbf{k}) \equiv \frac{1}{N_c} \langle q_{\mathbf{k}} q_{-\mathbf{k}} \rangle, \quad (5)$$

where  $q_{\mathbf{k}} = \sum_i e^{i\mathbf{k} \cdot \mathbf{r}_i} (n_i - f)$  is the Fourier transform of the charge distribution,  $\mathbf{k} = k_1 \mathbf{b}_1 + k_2 \mathbf{b}_2$  are the allowed wave vectors, with  $\mathbf{b}_1 = 2\pi\hat{x} - \frac{2\pi}{\sqrt{3}}\hat{y}$  and  $\mathbf{b}_2 = \frac{4\pi}{\sqrt{3}}\hat{y}$  the basis vectors of the reciprocal lattice to the grid, and  $k_i = l_i/L_i$  with  $l_i = 0, \dots, L_i-1$ . We also consider the real space correlations,

$$C(m_1, k_2) \equiv \frac{1}{L_1} \sum_{k_1} e^{-ik_1 m_1} S(k_1, k_2) \quad (6)$$

as well as  $C(k_1, m_2)$  defined similarly, and the 6-fold (hexatic) orientational order parameter  $\langle \Phi_6 \rangle$ , where

$$\Phi_6 \equiv \frac{1}{N_c} \sum_i \frac{1}{z_i} \sum_j e^{6i\theta_{ij}}. \quad (7)$$

In the above, the first sum is over all charges  $n_i = 1$ , the second sum is over all charges  $n_j = 1$  that are nearest neighbors of  $n_i$  (as determined by a Delaunay triangulation),  $z_i$  is the number of these nearest neighbors, and

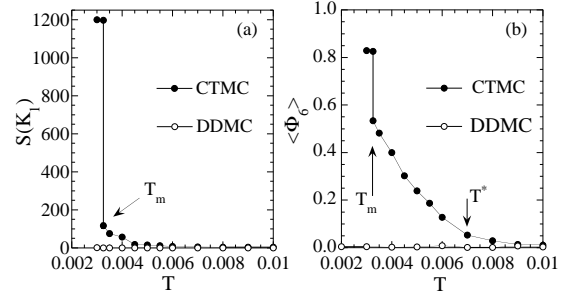


FIG. 1: (a) Plot of structure function transverse peak height  $S(\mathbf{K}_1)$ ,  $\mathbf{K}_1 = \frac{1}{5}\mathbf{b}_2$ , vs.  $T$ , and (b) hexatic order parameter  $\langle \Phi_6 \rangle$  vs.  $T$ , at fixed  $\mathbf{F} = 0.1\hat{x}$ , for both DDMC and CTMC algorithms.

$\theta_{ij}$  is the angle of the bond from  $n_i$  to  $n_j$  with respect to the  $\hat{x}$  axis.

The direct computation of  $S(\mathbf{k})$  and  $\langle \Phi_6 \rangle$  as in Eq.(4) is too costly as it involves lengthy calculations at each step of the simulation. Instead we approximate the integral in Eq.(4) by a Monte Carlo evaluation, choosing  $N_{\text{config}} \simeq 1000$  random times uniformly distributed over the simulation interval  $t \in [0, \tau]$  and averaging over the configurations at these times only.

We now present our results. Starting in the ground state at  $T = 0$ , the charge lattice remains pinned until the driving force  $F$  exceeds the change in interaction energy associated with moving one charge forward one grid space parallel to  $\mathbf{F}$ . This defines the  $T = 0$  critical force,  $F_c = 0.063$ , for both DDMC and CTMC. Our simulations are carried out for fixed  $F = 0.1$  as we vary  $T$ . Our results reported here are for a system size of  $L_1 = 500$  and  $L_2 = 60$ , with  $N_c = 1200$  charges. The reason for such an extreme aspect ratio will be discussed later. At  $F = 0$ ,  $T < T_m$ , the system forms an ordered triangular charge solid, and  $S(\mathbf{k})$  has sharp Bragg peaks at reciprocal lattice vectors  $\{\mathbf{K}\}$ . Let  $\mathbf{K}_1 = \mathbf{b}_2/5$  be smallest non-zero reciprocal lattice vector directed transverse to  $\mathbf{F}$ . In Fig. 1a we plot  $S(\mathbf{K}_1)$  vs.  $T$ , at  $F = 0.1$ , for both DDMC and CTMC. In Fig. 1b we plot  $\langle \Phi_6 \rangle$  vs.  $T$ . The results for DDMC show *no structure whatever* for the moving steady state. A plot in Fig. 2a of the full  $S(\mathbf{k})$  at  $T = 0.003$  shows an isotropic liquid. In fact, we find with DDMC that once the charged solid depins from the grid, the moving steady state is an isotropic liquid virtually everywhere in the  $F - T$  plane.

To see why this is so, consider a large  $F \gg F_c$  at  $T = 0$ , starting from an ordered solid. The DDMC picks a charge at random, then picks a direction to move it in at random; the move is accepted only if it lowers the energy, i.e. if the charge advances in the direction of  $\mathbf{F}$ . Since only 3 of the 6 possible directions do so, the move is accepted with probability 1/2. If the work done by the force dominates the interaction energy (as it should for

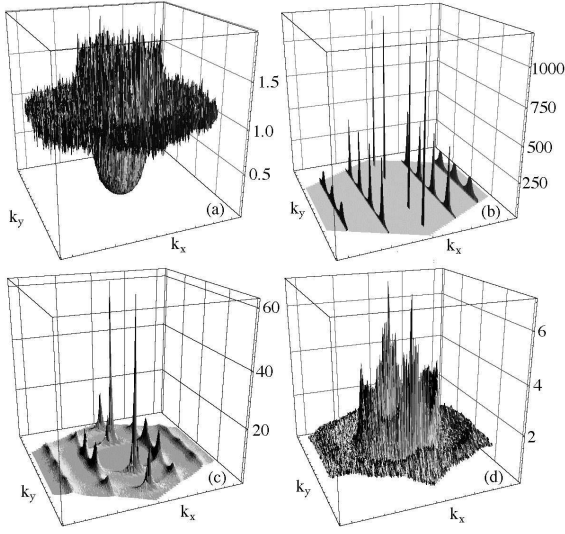


FIG. 2: Structure function  $S(\mathbf{k})$ , for  $\mathbf{k}$  in the first Brillouin zone, at force  $\mathbf{F} = 0.1\hat{x}$  for (a)  $T = 0.003$  with DDMC algorithm; and (b)  $T = 0.003$ , (c)  $T = 0.004$ , (d)  $T = 0.007$  with CTMC algorithm.

$F \gg F_c$ ) then after one pass a random half of all charges have moved forward. On the next pass, a different random half move forward. After several passes, the charges are completely disordered. Although this argument assumed  $F \gg F_c$ , we find that at  $T = 0$  the charges melt to a liquid at all  $F \geq F_c$ . The randomness of choosing proposed moves thus has a dramatic effect on the steady state order. In contrast, in CTMC, moves are chosen according to a probabilistic distribution which sharpens dramatically as  $T$  decreases. Unlikely moves are almost never chosen, and favorable moves are almost always chosen. The result, shown in Fig. 1, is more structure in the moving steady states. The rest of this work, therefore, focuses on CTMC.

For CTMC, the results of Fig. 1 show a discontinuous melting transition at  $T_m = 0.00325$ . In Fig. 2b–d we show representative plots of  $S(\mathbf{k})$  above and below  $T_m$ . We first consider  $T > T_m$ . Although the plot of  $S(\mathbf{k})$  at  $T = 0.004$  in Fig. 2c shows sharp peaks at the reciprocal lattice vectors of the ordered charge lattice, the magnitude of these peaks is greatly reduced from those at  $T < T_m$  (see Fig. 2b). We have carried out simulations for a larger system,  $L_2 = 120$ ,  $L_1 = 500$  and found  $S(\mathbf{k})$  to remain unchanged. This lack of finite size dependence in  $S(\mathbf{k})$  indicates that the system is a liquid with short ranged translational order. The peaks in  $S(\mathbf{k})$  result from large but finite correlation lengths. Similar behavior was seen in simulations of vortices in a square Josephson junction array with *random* pinning [13]; the prominent peaks at the transverse wavevectors along the  $k_y$  axis led those authors to denote this state as a “short ranged smectic”.

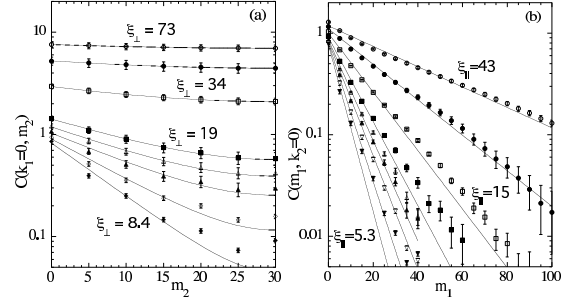


FIG. 3: (a) Transverse real space correlation  $C(k_1 = 0, m_2)$  vs.  $m_2$ , and (b) longitudinal real space correlation  $C(m_1, k_2 = 0)$  vs.  $m_1$ . Solid lines are fits to  $e^{-m/\xi} + e^{-(L-m)/\xi}$  and determine the correlation lengths  $\xi_\perp$  and  $\xi_\parallel$ . Curves from top to bottom are for  $T = 0.00325, 0.0035, 0.004, 0.0045, 0.005, 0.0055, 0.006, 0.007$ ;  $F = 0.1$ . Representative values for  $\xi_\perp$  and  $\xi_\parallel$  are shown.

To estimate the correlations lengths we plot in Fig. 3a,b  $C(k_1 = 0, m_2)$  vs.  $m_2$  and  $C(m_1, k_2 = 0)$  vs.  $m_1$ ; the first gives the decay of correlations in real space along  $\hat{a}_2$  (averaged over the direction  $\hat{a}_1$ ), while the second gives the decay of correlations along  $\hat{a}_1$ , parallel to the force  $\mathbf{F}$  (averaged over  $\hat{a}_2$ ). We plot only the values at integer multiples of the average particle spacing  $a_v = 1/\sqrt{F} = 5$ ; these define the upper envelop of the damped oscillating correlations. Fitting the data to the simple periodic decay  $C \sim e^{-m/\xi} + e^{-(L-m)/\xi}$  (where we use  $L_1$  or  $L_2$  as appropriate) gives the correlation lengths perpendicular,  $\xi_\perp$ , and parallel,  $\xi_\parallel$ , to the driving force  $\mathbf{F}$ . Representative values for  $\xi_\perp$  and  $\xi_\parallel$  are shown in Fig. 3 with  $\xi_\perp \sim 2\xi_\parallel$  near  $T_m$ . For Fig. 3b our fit is only to points  $m_1 > \xi_\parallel$ .

Although the liquid above  $T_m$  lacks translational order, Fig. 1b shows that hexatic orientational order grows for  $T < T^* \sim 0.007$ . Similar hexatic liquids have been reported in continuum simulations with *random* pinning [12]. In our case, the periodic triangular grid breaks rotational symmetry and in principle gives finite hexatic order at any  $T$ . It is unclear whether the onset of growing hexatic order at  $T^*$  is just this grid induced effect, increasing as the correlations lengths grow larger than the interparticle spacing,  $\xi > a_v$ , or whether it is a crossover remnant of what might be a true hexatic transition in another geometry.

Next we consider  $T < T_m$ .  $S(\mathbf{k})$  for  $T = 0.003 < T_m$  is shown in Fig. 2b. First we note that the peaks at  $\mathbf{K}$  on the  $k_y$  axis (at  $k_1 = 0, k_2 = 1/5, 2/5$ ) are sharp  $\delta$ -function Bragg peaks of height  $S(\mathbf{K}) \simeq N_c = 1200$ . We have computed the height of these peaks for smaller size systems and find that they scale  $\sim N_c$ . This indicates that this state has long range smectic order; the particles are confined to periodically spaced channels parallel to the driving force. Next, we note that the peaks at finite  $k_x$  (at  $k_1 = 1/5, 2/5$ ) are essentially  $\delta$ -functions in  $k_x$ . Sim-

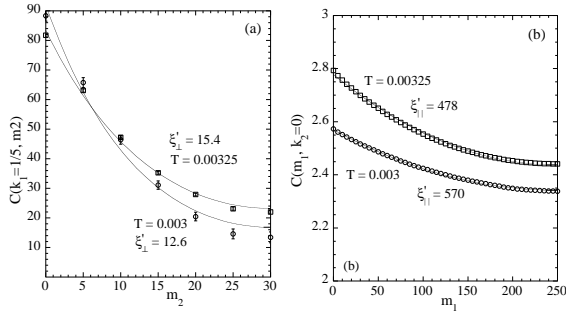


FIG. 4: (a) Transverse correlation between the smectic channels,  $C(k_1 = 1/5, m_2)$  vs.  $m_2$ , and (b) longitudinal correlation  $C(m_1, k_2 = 0)$  vs.  $m_1$ , in the smectic state for  $T = 0.003, 0.00325 \leq T_m$ ,  $F = 0.1$ . Solid lines are fits to  $e^{-m/\xi} + e^{-(L-m)/\xi}$  and determine the correlation lengths  $\xi'_\perp$  and  $\xi'_\parallel$ .

ulations for smaller size systems show that the height of these peaks scale  $\sim L_1$ . This indicates that the particles are perfectly ordered within each smectic channel. The finite width of these peaks, as  $k_y$  varies, indicates that the ordered channels are randomly displaced with respect to each other, with a finite correlation length  $\xi'_\perp$ . To determine this correlation length we plot in Fig. 4a  $C(k_1 = 1/5, m_2)$  vs.  $m_2$  and fit to a periodic decay as earlier. Finally we return to the issue of the longitudinal order in the smectic state. Since the transverse order among the smectic channels is short ranged, with finite  $\xi'_\perp$ , we can regard the channels as decoupled one dimensional systems. Thus only short ranged longitudinal order should be expected. We have investigated this issue by carrying out detailed finite size analyses on smaller size systems. We conclude that the smectic does in fact have a finite longitudinal correlation length  $\xi'_\parallel$ , but that  $\xi'_\parallel \gtrsim L_1$ ; we find that when the system length is increased so that  $\xi'_\parallel \lesssim L_1$ , the smectic becomes unstable to the liquid. In Fig. 4b we plot the longitudinal correlation  $C(m_1, k_2 = 0)$  vs.  $m_1$  for  $T = 0.003, 0.00325$  just below  $T_m$ . Fitting to the periodic exponential decay assumed earlier, we find  $\xi'_\parallel \sim 500$ . For a smaller length,  $L_1 = 120$ , the smectic persisted up to the higher  $T = 0.006$ . Our desire to suppress  $T_m$  to low temperatures, so as to see growing correlations in the liquid, was the reason we chose  $L_1 = 500$  for the simulations reported on here. While the smectic thus disappears in the true thermodynamic limit, since  $\xi'_\parallel$  grows exponentially as  $T$  decreases, the smectic will ultimately appear in a finite sized system at sufficiently low  $T$ . We find that once  $\xi'_\parallel \gtrsim L_1$ , the smectic is the stable state of the system; for  $L_1 = L_2 = 120$ , we have succeeded in cooling into the smectic from the disordered liquid. Our observation of a smectic state on finite length scales, which becomes unstable to a liquid on large length scales, agrees in part with arguments in Ref. [9].

Interacting 2D vortices in a periodic potential at finite temperature have been simulated by several others using *continuum* dynamics. The molecular dynamic simulations of Reichhardt and Zimányi [15] and Carneiro [16] used square periodic pins embedded in a flat continuum, with a number of vortices equal to, or greater than, the number of pins. Such models cannot be well described by our discrete grid. Closer to our model is that of Marconi and Domínguez [17] who simulate the RSJ dynamics of a vortex density  $f = 1/25$  in a *square* Josephson array, and find an ordered moving vortex lattice. However in their case, the energy to move a single vortex forward from its ground state position is  $\Delta E_1 \simeq 0.34$ , whereas the energy barrier between cells of the array is  $U_0 \simeq 0.12$ . The parameters of our simulations, which assume  $\Delta E_1 < F < U_0$  (see discussion preceding Eq. (5)), are therefore in a more strongly pinned limit outside the range of their model. It therefore remains for future investigation to test if the results of the CTMC method agree with that of continuum models in the corresponding limit.

We wish to thank D. Domínguez, M. C. Marchetti and A. A. Middleton for helpful discussions. This work was supported by DOE grant DE-FG02-89ER14017 and NSF grant PHY-9987413.

---

\* present address: Department of Physics, MIT

- [1] B. Schmittmann, and R. K. P. Zia, in *Phase Transitions and Critical Phenomena*, v.17, C. Domb and J. L. Lebowitz, eds. (Academic, 1995).
- [2] S. Katz, J. L. Lebowitz and H. Spohn, Phys. Rev. B **28**, 1655 (1983); J. Stat. Phys. **34**, 497 (1984).
- [3] A. B. Bortz, M. H. Kalos and J. L. Lebowitz, J. Comp. Phys. **17**, 10 (1975).
- [4] M. E. J. Newman and G. T. Barkema, *Monte Carlo Methods in Statistical Physics*, (Clarendon, 1999); J. Dall and P. Sibani, Comp. Phys. Comm. **141**, 260 (2001).
- [5] M. Franz and S. Teitel, Phys. Rev. B **51**, 6551 (1995).
- [6] S. Teitel, Phys. Rev. B **39**, 7045 (1989).
- [7] V. Ambegaokar and B. I. Halperin, Phys. Rev. Lett. **22**, 1364 (1969).
- [8] T. Giamarchi and P. Le Doussal, Phys. Rev. Lett. **76**, 3408 (1996); P. Le Doussal and T. Giamarchi, Phys. Rev. B **57**, 11356 (1998).
- [9] L. Balents, M. C. Marchetti and L. Radzihovsky, Phys. Rev. Lett. **78**, 751 (1997); Phys. Rev. B **57**, 7705 (1998).
- [10] S. Scheidl and V. M. Vinokur, Phys. Rev. E **57**, 2574 (1998).
- [11] A. E. Koshelev and V. M. Vinokur, Phys. Rev. Lett. **73**, 3580 (1994); M. C. Faleski, M. C. Marchetti and A. A. Middleton, Phys. Rev. B **54**, 12427 (1996); K. Moon, R. T. Scalettar and G. T. Zimányi, Phys. Rev. Lett. **77**, 2778 (1996).
- [12] S. Ryu, M. Hellergqvist, S. Doniach, A. Kapitulnik and D. Stroud, Phys. Rev. Lett. **77**, 5114 (1996); S. Spencer and H. J. Jensen, Phys. Rev. B **55**, 8473 (1997).
- [13] D. Domínguez, Phys. Rev. Lett. **82**, 181 (1999);

- A. B. Kolton, D. Domínguez and N. Gronbech-Jensen, Phys. Rev. Lett. **83**, 3061 (1999).
- [14] H. Fangohr, S. J. Cox and P. A. J. de Groot, Phys. Rev. B **64**, 064505 (2001).
- [15] C. Reichhardt and G. T. Zimányi, Phys. Rev. B **61**, 14354 (2000).
- [16] G. Carneiro, Phys. Rev. B **62**, R14661 (2000); *ibid.* **66**, 054523 (2002).
- [17] V. I. Marconi and D. Domínguez, Phys. Rev. Lett. **82**, 4922 (1999); Phys. Rev. B **63**, 174509 (2001).